ISSN (Print) 1226-1750
ISSN (Online) 2233-6656
Journal of Magnetics 25(4), 670-673 (2020) https://doi.org/10.4283/JMAG.2020.25.4.670

Development of DOI Detector for PET using Different Kinds of Reflectors

Seung-Jae Lee[1,2] and Cheol-Ha Baek[3]*

[1]*Department of Radiological Science, Dongseo University, Busan 47011, Republic of Korea*
[2]*Center for Radiological Environment & Health Science, Dongseo University, Busan 47011, Republic of Korea*
[3]*Department of Radiological Science, Kangwon National University, Gangwon 25949, Republic of Korea*

(Received 22 October 2020, Received in final form 11 December 2020, Accepted 11 December 2020)

We developed a depth of interaction (DOI) detector for positron emission tomography (PET) using different kinds of reflectors. The detector module consists of two layers of scintillator arrays, which was composed of 4 × 4 Gadolinium Aluminum Gallium Garnet (GAGG) crystals of size 3 mm × 3 mm × 10 mm, and 4 × 4 silicon photomultiplier (SiPM) arrays. The bottom layer optically coupled to the SiPM used a diffuse reflector and the top layer used a specular reflector. The layer interacted with gamma ray and crystal could be determined by analyzing the signal size because it obtained for each layer is different by using different reflectors for the crystals for each layer. The detector performance was analyzed by the flood image, energy spectrum with two photoelectric peaks, and energy resolution. In the experiment for the detector module performance, all pixels in the flood map were well decoded, and the energy spectrum of each pixel is measured with two photo peaks.

Keywords : Positron Emission Tomography (PET), Depth of Interaction (DOI), reflectors, energy spectrum, Magnetic Resonance Imaging (MRI)

1. Introduction

Positron emission tomography (PET) requires high resolution and sensitivity in order to acquire a lot of biometric and accurate information in various studies of humans and animals [1, 2]. Various devices have been developed to meet these requirements for small animal imaging, and organ specific imaging such as a human brain [3-5]. The characteristics of these systems use small gantry for high sensitivity, and thin and long scintillator for high resolution [6]. Because these crystals shape increase the fraction of gamma rays obliquely incident on the detector surface, the spatial resolution gradually degrades from the center to the periphery of the field of view (FOV) due to the parallax errors [7-9]. The depth of interaction (DOI) detector, which acquires information regarding the depth of gamma interaction in the crystal pixels has been developed to solve these problems [10-14]. However, these methods still have certain technical challenges and performance trade-offs [15].

The aim of this study was to develop a novel and simple DOI detector that composed of two layers of crystal arrays and one photo sensor array. The proposed detector uses different kinds of reflectors in each layer, so that on the energy spectrum appears two photoelectric peaks corresponding to each layer crystal. The layer interacted with gamma ray and crystal could be determined by analyzing the energy spectrum. Experimental measurements were performed to investigate the DOI capability of the proposed detector.

2. Experimental Details

2.1. Detector configuration

The detector consists of two layers of scintillator arrays, and one silicon photomultiplier (SiPM) as a photo sensor array. Figure 1 shows a schematic diagram of the DOI detector. Scintillators were used with Gadolinium Aluminum Gallium Garnet (GAGG) [16], which were made of arrays of two layers with different reflectors as shown in Fig. 2. GAGG has a density of 6.63 g/cm^3, and has a high energy resolution by generating a large number of lights, such as 50,000 photons/MeV. In addition, since the scintillator itself does not generate natural radiation, GAGG has excellent characteristics that do not affect the signal to be measured. The size of each crystal pixel was

*Corresponding author: Tel: +82-33-540-3384
Fax: +82-33-540-3389, e-mail: baekch@kangwon.ac.kr

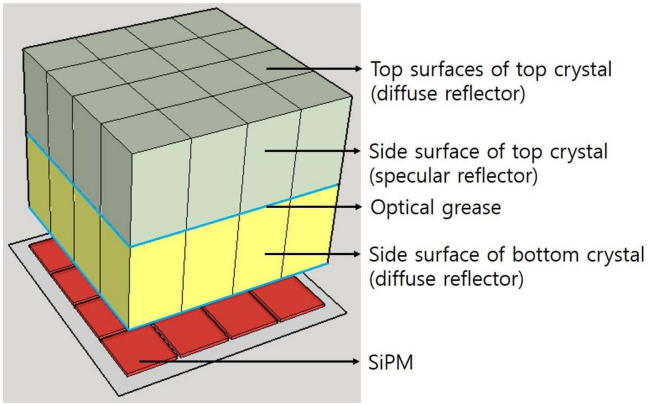

Fig. 1. (Color online) Schematic diagram of the two layer DOI detector. The blue line represents the optical grease, which is used between the crystal layers and between the crystal and the SiPM.

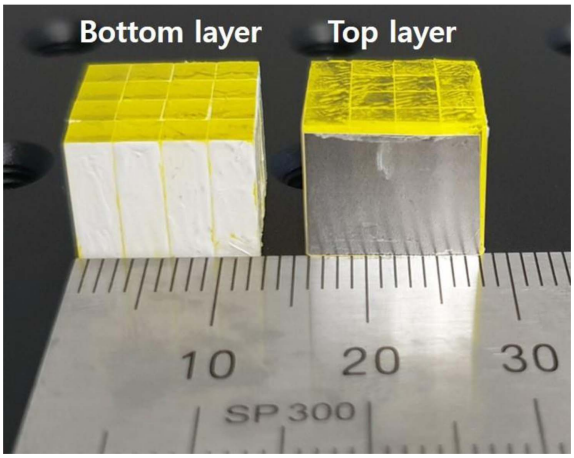

Fig. 2. (Color online) Configuration of GAGG scintillator with diffuse and specular reflectors.

3 mm × 3 mm × 10 mm, and was composed of two layers in 4 × 4 array. Optical grease was used between the crystal layers, and the crystal layer and the SiPM to prevent the reduction of light transmission due to a sudden change in refractive index.

The side surfaces of crystal pixel in the top layer used specular reflectors with the same incident angle and reflectance angle when reflecting the light generated by the interaction between the gamma rays and the crystal, and it of bottom layer and the top surfaces of the top layer crystals used diffuse reflectors with random reflection. The specular reflector used enhanced specular reflector (ESR) with 98 % reflectivity [17], and the diffuse reflector used BC-620 reflective paint [18] with reflectance greater than 95 %. MatrixSM-9 system was used to detect the light generated from the crystals, and the SiPM pixel size

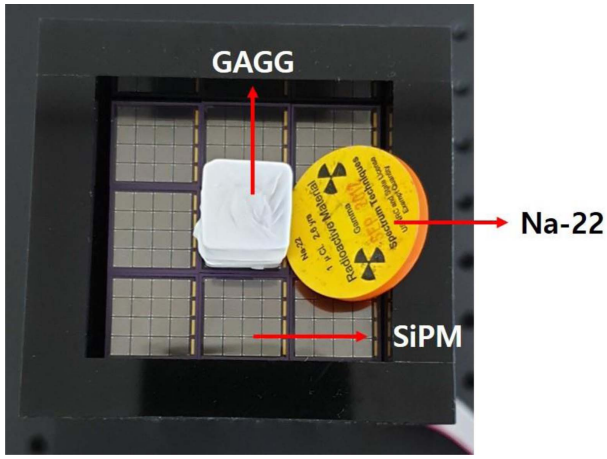

Fig. 4. (Color online) Experimental set-up. The data was acquired by using a Na-22 point source.

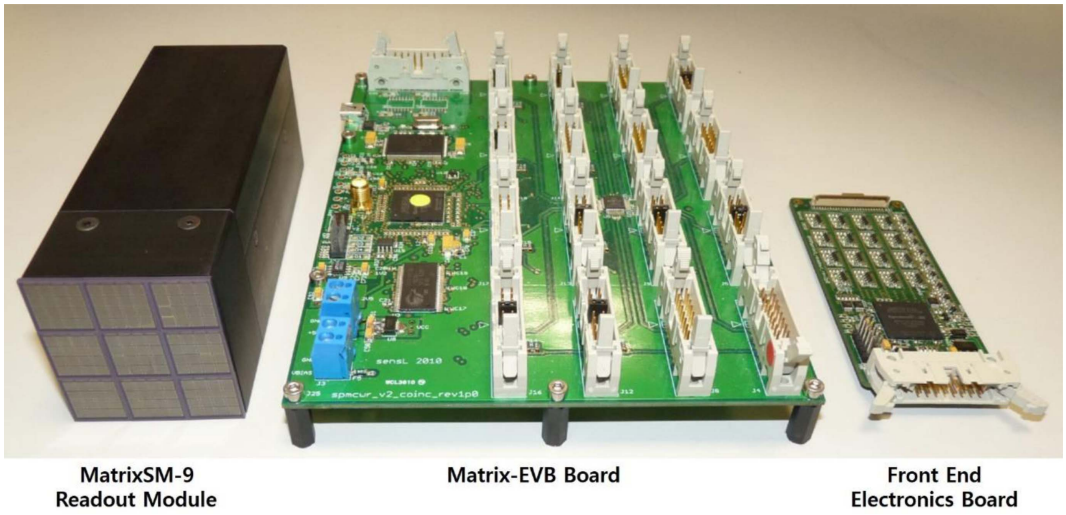

Fig. 3. (Color online) MatrixSM-9 system. The system consists of the readout module with the front end electronics board, and Matrix-EVB board as a mainboard to process and transport the signal.

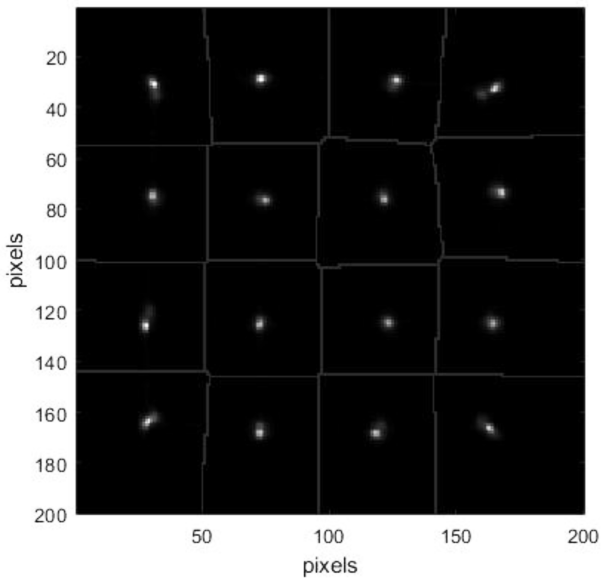

Fig. 5. Flood map with segmented pixels for the DOI detector.

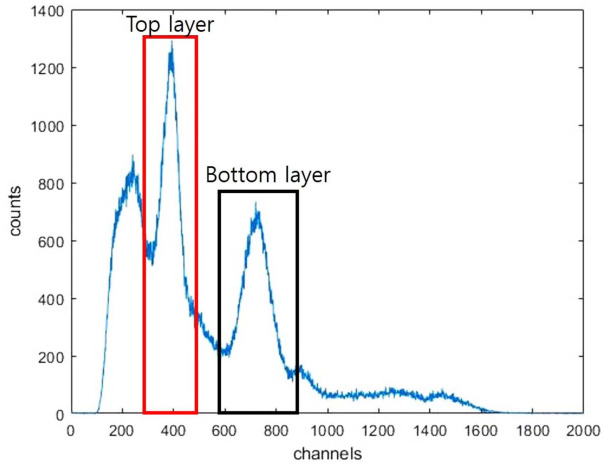

Fig. 6. (Color online) Global energy spectrum for the DOI detector with two layer of crystals.

is 3 mm × 3 mm, with a pitch of 3.37 mm in a 4 × 4 array. This system consists of the readout module with the front end electronics board, and Matrix-EVB board as a mainboard to process and transport the signal as shown in Fig. 3 [19].

2.2. Experimental Set-up

A flood image and energy spectrum were acquired using Na-22 point source (~0.15 μCi) that emits positrons to generate gamma rays of 511 keV. In order to represent the position of each crystal pixel in the flood image with similar counts, data were obtained by placing a source on each side of the crystal array as shown in Fig. 4. The 16 channels of data were reduced to 4 channels using the Anger equation to reconstruct the image.

3. Results and Discussion

Flood images were reconstructed using the Anger equation with data from Na-22 sources obtained in all

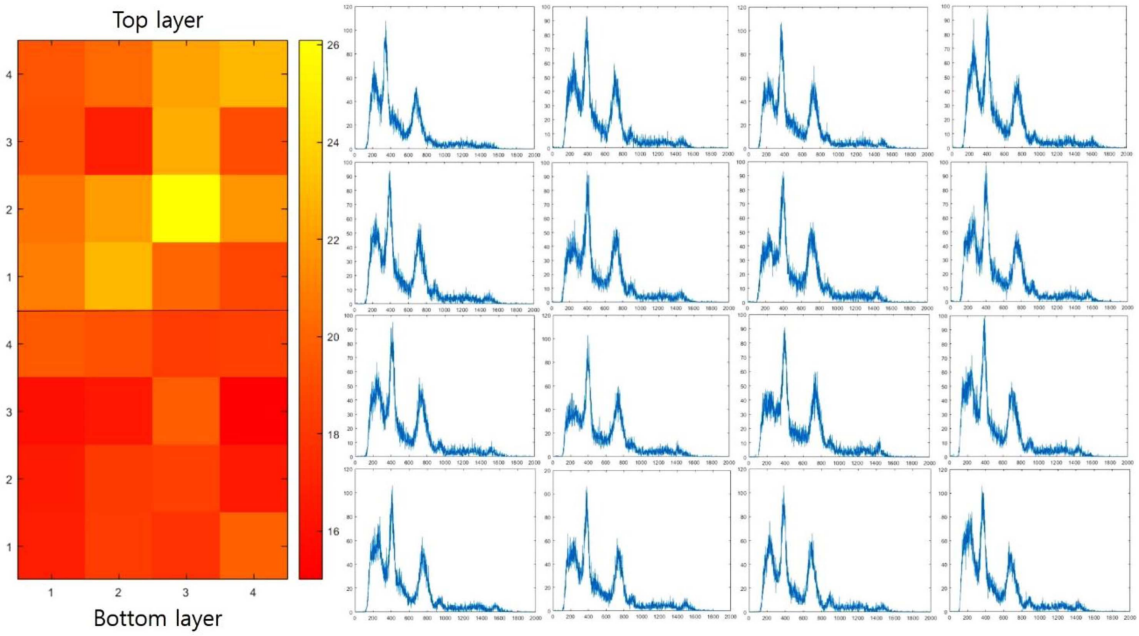

Fig. 7. (Color online) Energy resolution distribution (left) and energy spectra (right) corresponding to each pixel position in the flood image.

direction of the crystal block. Figure 5 shows the flood map of a 4 × 4 crystal array of two layers. All pixels were clearly segmented, and composed of two layers but were acquired as a single point image in every pixel.

The energy spectrum was measured using the obtained data. Figure 6 shows the global energy spectrum, and it can be seen that two photoelectric peak of 511 keV were clearly seen. The lower channel photoelectric peak of the two photoelectric peak is the peak of gamma rays detected in the crystal of the top layer, and the photoelectric peak of the high channel is the peak of gamma rays detected in the crystal of the bottom layer. The energy resolution of each photoelectric peak at the global energy spectrum was 19.8 % (bottom layer) and 23.8 % (top layer), respectively. Figure 7 shows the energy resolution distribution of the flood image and energy spectra that correspond to each crystal position of the flood image. Two photoelectric peaks are also identified in the energy spectrum acquired at each crystal position. Since the distribution of the photoelectric peak is clearly distinguished, the crystal of the layer interacted with gamma rays can be completely separated. The energy resolution of the bottom layer was measured on average 17.9 % with a range of 15.0 % to 20.0 %, and it of the top layer averaged 21.0 % in the range of 16.9 % to 26.1 %.

4. Conclusion

In this study, we developed the detector that measures the interaction depth using two layers of the scintillator pixel arrays with different reflectors. The bottom layer uses the specular reflector and the top layer uses the diffuse reflector to vary the size of the light signal obtained from the SiPM. The signal size of the light obtained is different for each layer, where the channel positions of the photoelectric peaks appear elsewhere on the energy spectrum. In the flood image, the position of each scintillator pixel is imaged at the same position irrespective of the layers, so that it is difficult to classify the layers. However, the positions of the photoelectric peaks on the energy spectrum appear in different channels, so performing photoelectric peak analysis of the energy spectrum can distinguish the layers. By specifying the two energy ranges to be obtained at the detector, the layers can be separated very easily and simply.

When the proposed detector is applied to PET detector that acquires specific organ images such as the human brain, and small animal images, it is possible to measures the depth position where gamma rays and scintillators interact. Thus, it will be possible to solve the parallax errors reducing the spatial resolution.

Acknowledgments

This research was supported by the National Foundation of Korea (NRF) funded by the Ministry of Education, Science and Technology (2020R1C1C1004584).

References

[1] C. Catana, J. Nucl. Med. **60**, 8 (2019).
[2] E. Yoshida, K. Kitamura, T. Tsuda, K. Shibuya, T. Yamaya, N. Inadama, T. Hasegawa, and H. Murayama, Nucl. Inst. Meth. A **557**, (2006).
[3] Y. C. Tai, A. Chatziioannou, S. Siegel, J. Young, D. Newport, R. N. Goble, R. E. Nutt, and S. R. Cherry, Phys. Med. Bio. **46**, 7 (2001).
[4] Y. C. Wang, J. Seidel, B. M. W. Tsui, J. J. Vaquero, and M. G. Pomper, J. Nucl. Med. **47**, 11 (2006).
[5] Q. Bao, D. Newport, M. Chen, D. B. Stout, and A. F. Chatziioannou, J. Nucl. Med. **50**, 3 (2009).
[6] H. Peng and C. S. Levin, Curr. Pharm. Bio. **11**, 6 (2010).
[7] R. S. Miyaoka, T. K. Lewellen, H. Yu, and D. L. McDaniel, IEEE Trans. Nucl. Sci. **45**, 3 (1998).
[8] S. E. Derenzo, W. W. Moses, H. G. Jackson, B. T. Turko, J. L. Cahoon, A. B. Geyer, and T. Vuletich, IEEE Trans. Nucl. Sci. **36**, 1 (1989).
[9] W. W. Moses, S. E. Derenzo, C. L. Melcher, and R. A. Manente, IEEE Trans. Nucl. Sci. **42**, 1 (1995).
[10] K. C. Burr, A. Ivan, D. E. Castleberry, J. W. LeBlanc, K. S. Shah, and R. Farrell, IEEE Trans. Nucl. Sci. **51**, 4 (2004).
[11] Y. Shao, X. Sun, K. A. Lan, C. Bircher, K. Lou, and Z. Deng, Phys. Med. Biol. **59**, 5 (2014).
[12] S. Salvador, D. Huss, and D. Brasse, IEEE Trans. Nucl. Sci. **56**, 1 (2009).
[13] S-J. Lee and C-H. Baek, Nucl. Inst. Meth. A **887**, (2018).
[14] S-J. Lee and C-H. Baek, J. Kor. Phy. Soc. **73**, (2018).
[15] M. Ito, S. J. Hong, and J. S. Lee, Bio. Eng. Lett. **1**, (2011).
[16] http://www.epic-crystal.com/oxide-scintillators/gagg-ce-scintillator.html
[17] http://multimedia.3m.com/mws/media/1389248O/application-guide-for-esr.pdf
[18] http://static6.arrow.com/aropdfconversion/5f21e5069a452c0b4d6a95c9954f098ba 0ad6261/113423053200175sgc-bc620-data-sheet_.pdf
[19] http://www.sensl.com/downloads.ds/PB-MatrixB.pdf